Electronic Supplementary Material (ESI) for Nanoscale.

Untangling the physics of water transport in Boron Nitride nanotubes†

S. Mistry, R. Pillai, D. Mattia and M. K. Borg

1 Molecular dynamics simulations

We carried out the simulations using the molecular dynamics (MD) open source software LAMMPS [1]. Two different setups are studied. Setup 1 consists of a short membrane, with a reservoir of water on each side and a nanotube embedded within the graphene or BN sheets connecting the two reservoirs. Setup 2 is a periodic nanotube, essentially modelling a tube of infinite length. Both setups are shown in Fig. 1.

1.1 Setup 1

This setup consists of two reservoirs on either side of a nanotube embedded in a nanosheet of the same material. Both reservoirs have the same dimensions: 40 Å, 80.94 Å and 81.1639 Å in the x, y and z directions, respectively. The y and z dimensions were chosen to make sure the graphene/BN sheets were periodic. The nanotube length was set as 200.45 Å, which ensures that they contain enough water molecules to obtain a steady state value of density within the tube.

The absolute pressure in the upstream reservoir was set to 200 MPa, while the downstream reservoir was set to 0.1 MPa. Corresponding values for density was taken from the NIST database [2].

1.2 Setup 2

The second setup consisted of periodic tubes, essentially modelling infinitely long nanotubes. For the CNTs, we replicated the nanotube lengths as in Borg *et al.* [3] For BNNTs, the charges on the nanotube surface made the simulations computationally expensive, with more than 90% of the time spent in long range Coulombic calculations. We therefore reduced the nanotube length by half for BNNTs. We filled the nanotubes with water using densities measured from setup 1. Here we use the same definition of diameter in the calculation of volume for both the setups. One could equivalently use the number of molecules per unit length. The lengths of the BNNT and CNT nanotubes are given in Table 1.

Table 1 Nanotube dimensions for Setup 2

Chirality	CNT Length (Å)	BNNT Length (Å)	D (nm)
(6,6)	3153.1	1576.54	0.81
(7,7)	3153.1	1576.54	0.95
(8,8)	1576.54	787.044	1.08
(10,10)	1576.54	787.044	1.36
(15,15)	314.81	314.81	2.03
(30,30)	157.4	157.4	4.07

The nanotubes were created by repeating a unit cell consisting of carbon for CNTs and boron/nitrogen atoms for BNNTs, respectively, and then rolling them according to the desired chirality. In our simulations, the CNTs and the BNNTs share the same diameters. Literature uses BN bond lengths that vary between 1.43 Å to 1.46 Å [4,5] which increases their diameters by 0.2–0.4 Å compared to CNTs. However, for our study we have kept the bond lengths for the C-C and the B-N bonds constant at 1.42 Å to remove any differences in flow resistances which might arise due to the different diameters of the nanotubes, although we verify that changing the bond length for BNNT to 1.44 Å has a negligible effect on the transport of water.

1.3 Partial charges

The partial charges used for BNNTs, presented in Table 2, is not consistent within the literature. Won *et al.* [6] present a number of charges ranging from ±0.4e to ±1.05e, depending on the nanotube radius and whether it was filled or empty. Hilder *et al.* [7] have noted that it is not clear what charges should be used for the BNNTs. They use two values of ±0.4e and ±1.05e. Liang [8] used ±0.3e, Sam *et al.* [9] used ±0.35 while Ritos *et al.* [10] used ±1.05e. Largely, the two most used values are either ±0.3e or ±1.05e, and others deviate slightly from these. Both Won *et al.* [6] and Hilder *et al.* [11] suggest the higher partial charge of ∼±1e when the nanotube is filled with water, and ∼±0.3e when it is empty. Wu *et al.* [12], in contrast, suggests partial charge of ±0.3e for a sheet of BN atoms in contact with water.

Table 2 B-N partial charges in literature

Papers	Partial charge (±e)
Won [6]	0.4–1.05
Hilder [7], Ritos [10], Wei [13]	1.05
Casanova [14], This work	0.96
Hilder [11]	0.98
Hilder [7]	0.4
Sam [9]	0.35
Wu [12], Liang [8], Zhang [15]	0.3

For this study, we used the charge equilibration method as implemented within LAMMPS [16] to set charges on the BNNTs. We used the default parameters of electronegativity, self-Coulomb potential and the valence orbital exponent found in the REAXFF parametrization given by Han *et al.* [17]. We found that the charges obtained were fluctuating around ± 0.959e, which we then set to be constant for all BNNTs.

The TIP4P/2005 model [18] was used to simulate the water molecules. The O-H bond of the water molecules were restrained with the SHAKE algorithm [19]. The short range interactions were modelled in the form of a Lennard-Jones (LJ) potential. Coulombic interactions were carried out using the Particle-Particle Particle-Mesh (PPPM) method [20].

1.4 Lennard-Jones parameters

Interaction parameters from literature for the BNNTs are presented in Table 3. Note that earlier studies tend to use B,N-O interaction parameters given by Won *et al.* [6] , while recent studies use values

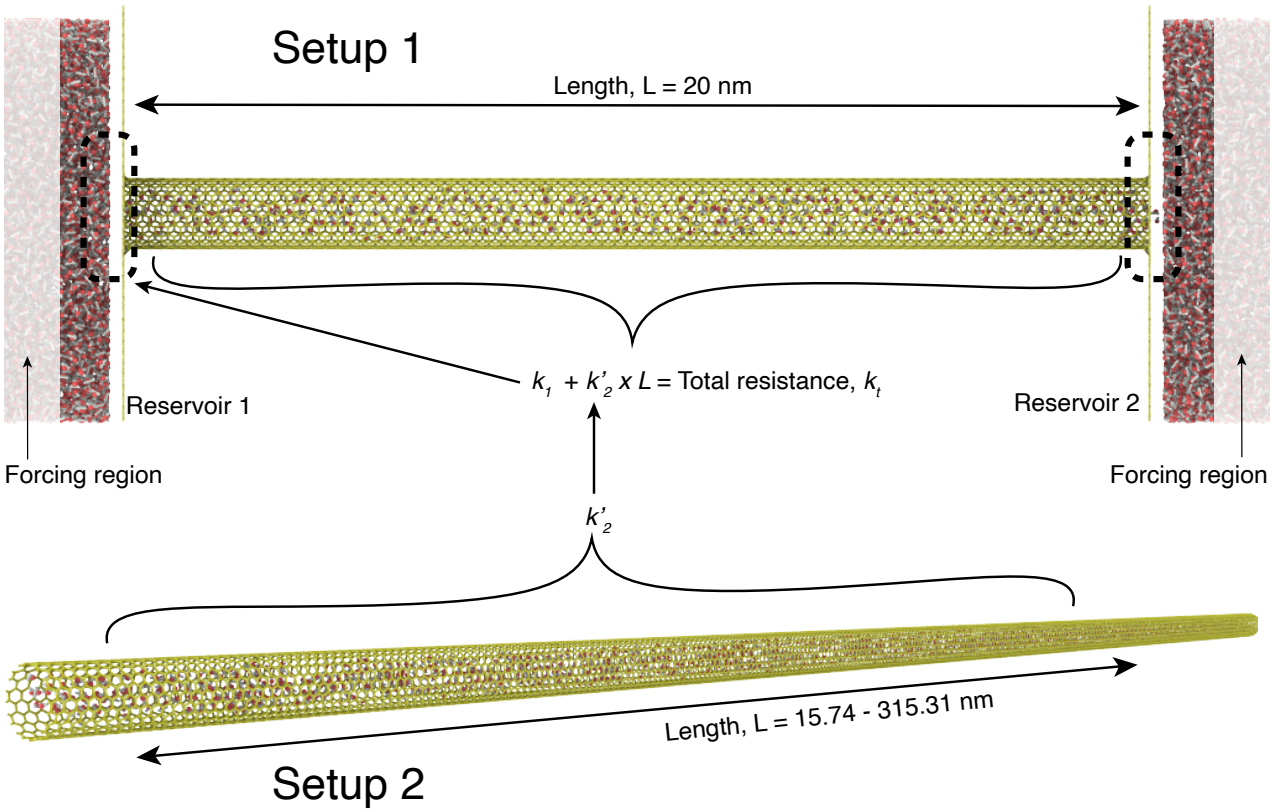

Fig. 1 Illustrated setup for our MD simulations. k_1 is the end resistance, k'_2 is the nanotube flow resistance per unit length and k_t is the total resistance. k'_2 is calculated from periodic simulation, and k_1 is calculated by subtracting $k'_2 \times L$ from k_t.

given by Wu *et al.*[12] For this study, we chose to use the LJ potentials provided by Wu *et al.*[12] as it is the more recent parametrization, and as we show later on, these potentials produced the experimentally-observed contact angles. Moreover, these potentials were derived from first principles using ab initio methods (diffusion Monte Carlo and random phase approximation) without the use of any fitting parameters. As noted by them, earlier potentials also significantly over predict wetting of BNNTs. As such, we also show later on that these potentials produced our experimentally-observed contact angles.

Table 3 Lennard-Jones interaction parameters in literature

Papers	ε_{BO} (kcal/mol)	ε_{NO} (kcal/mol)
Suk[21], Won[6], Hilder[7], Wei[13]	0.1214	0.1500
Wu[12], Liang[8], Zhang[15], Casanova[14]	0.0981	0.1213
Hilder[11]	0.2624	0.1757

Table 4 Lennard-Jones pair-potential parameters used in this study

Interaction pair	ε (kcal/mol)	σ (Å)
O-O	0.1852	3.159
C-O	0.1020	3.190
B-O	0.0981	3.322
N-O	0.1213	3.278
H-all	0	0

1.5 Runtime details

The equilibration run was carried out for 0.2 ns and the production run was > 3 ns for all the simulations. Temperature was maintained at 300 K in the reservoirs for setup 1 and in the nanotube for setup 2 using a Berendsen thermostat[22] with a damping parameter of 100 timesteps. No thermostat was applied to the water molecules inside the nanotube for setup 1.

For setup 1, the flow was driven by adding a constant force of 0.0208 kcal/mol to every oxygen atom in the forcing region shown in Fig. 1(a). This set up a pressure drop of $\Delta P = 200$ MPa across the nanotube. This value was determined using the equation:

$$F = \frac{1}{\rho_n}\frac{\Delta P}{\Delta L}, \tag{1}$$

where F is the force on each molecule, ρ_n is the number density measured in the forcing region, and $\Delta L = 40$Å is the length of the forcing region.

For setup 2, a constant force was added to all oxygen atoms within the nanotube (see Eqn. 1). The magnitude of this force was adjusted before the production runs such that the mean axial flow velocity $10 < v_x < 100$ m/s, to improve statistics in the measurements. We also check that the transport remains in the linear flow response regime by halving the force and verifying the flow velocity is also halved.

1.6 Post-processing details

For setup 1, the mass flow rate was calculated by counting the number of water molecules crossing a virtual plane set in the centre of the nanotube for the duration of the simulation. For setup 2, the mass flow rate was calculated by multiplying the mean velocity of all water molecules inside the nanotube with their total mass.

The density inside the nanotube for setup 1 was calculated for the central region of the nanotube by excluding 10 Å of the nanotube section from each end. This density was then used to determine the number of water molecules in setup 2. Densities inside the BNNTs and CNTs are similar to those found in Borg *et al.*[3]

The molecular residence time t_{res} for setup 1 was estimated by considering the trajectories of the molecules which crossed from one end of the nanotube to the other, across virtual planes set in both the reservoirs. These planes were placed at an adequate distance from the pore end to capture the flow physics at the pore, while excluding flow near the pistons. A cylindrical region of diameter $D-\sigma$ extending axially from inside the nanotube to the reservoir edges was considered. The t_{res} at a specific location is estimated by taking the average time spent at that location by each molecule which traversed across the two virtual planes. t_{res} provides a way of quantifying the local flow resistance in different regions of the membrane.

The 2-D density plots at the pore entrance were generated using cylindrical bins of 0.5 Å in the radial direction and 1 Å in the axial direction.

2 Results

2.1 Resistances for setup 1

Table 5 Results for CNTs: flow rates, applied pressure drop, measured total flow resistance

Chirality	$\dot{m}$ (kg/s)	ΔP (Pa)	k_t ($m^{-1}s^{-1}$)
(6,6)	8.15(±1.56)E-16	2.02E+08	2.48(±0.47)E+23
(7,7)	1.94(±0.07)E-15	2.02E+08	1.04(±0.04)E+23
(8,8)	2.27(±0.44)E-15	2.02E+08	8.89(±1.71)E+22
(10,10)	9.19(±0.52)E-15	2.02E+08	2.20(±0.12)E+22
(15,15)	4.54(±0.02)E-14	2.01E+08	4.43(±0.02)E+21
(30,30)	4.98(±0.03)E-13	2.01E+08	4.03(±0.03)E+20

Table 6 Results for BNNT-H: flow rates, applied pressure drop, measured total flow resistance

Chirality	$\dot{m}$ (kg/s)	ΔP (Pa)	k_t ($m^{-1}s^{-1}$)
(6,6)	4.04(±0.39)E-16	2.02E+08	5.00(±0.49) E+23
(7,7)	1.84(±0.16)E-15	2.02E+08	1.09(±0.09) E+23
(8,8)	2.55(±0.04)E-15	2.02E+08	7.92(±0.14) E+22
(10,10)	7.57(±0.17)E-15	2.02E+08	2.66(±0.06) E+22
(15,15)	3.66(±0.03)E-14	2.01E+08	5.50(±0.04) E+21
(30,30)	3.69(±0.03)E-13	2.01E+08	5.45(±0.04) E+20

Table 7 Results for BNNT: flow rates, applied pressure drop, measured total flow resistance

Chirality	$\dot{m}$ (kg/s)	ΔP (Pa)	k_t ($m^{-1}s^{-1}$)
(6,6)	2.76(±0.08)E-16	2.02E+08	7.32(±0.20) E+23
(7,7)	9.74(±0.16)E-16	2.02E+08	2.07(±0.03) E+23
(8,8)	1.42(±0.05)E-15	2.02E+08	1.42(±0.05) E+23
(10,10)	5.42(±0.08)E-15	2.02E+08	3.72(±0.05) E+22
(15,15)	2.33(±0.49)E-14	2.01E+08	8.63(±1.82) E+21
(30,30)	3.41(±0.01)E-13	2.01E+08	5.90(±0.02) E+20

Table 8 Results for BNNT – no charge: flow rates, applied pressure drop, measured total flow resistance

Chirality	$\dot{m}$ (kg/s)	ΔP (Pa)	k_t ($m^{-1}s^{-1}$)
(6,6)	6.75(±0.60)E-16	2.02E+08	2.99(±0.27) E+23
(7,7)	1.56(±0.06)E-15	2.02E+08	1.30(±0.05) E+23
(8,8)	1.37(±0.04)E-15	2.02E+08	1.47(±0.04) E+23
(10,10)	8.02(±0.13)E-15	2.02E+08	2.52(±0.04) E+22
(15,15)	4.43(±0.01)E-14	2.02E+08	4.55(±0.01) E+21
(30,30)	4.87(±0.02)E-13	2.01E+08	4.13(±0.01) E+20

2.2 Resistances for setup 2

Table 9 Results for CNT

Chirality	$\dot{m}$ (kg/s)	$\Delta P/\Delta L$ (Pa/m)	k_2' ($m^{-2}s^{-1}$)
(6,6)	1.08(±0.03)E-14	6.8817E+13	6.38(±0.20) E+27
(7,7)	2.44(±0.07)E-15	7.7628E+13	3.18(±0.09) E+28
(8,8)	1.01(±0.07)E-14	1.0305E+14	1.02(±0.07) E+28
(10,10)	5.81(±0.49)E-15	1.0258E+14	1.77(±0.15) E+28
(15,15)	1.41(±0.11)E-14	1.0929E+14	7.73(±0.60) E+27
(30,30)	8.57(±1.00)E-14	1.1448E+14	1.34(±0.16) E+27

Table 10 Results for BNNT q=0.0e

Chirality	$\dot{m}$ (kg/s)	$\Delta P/\Delta L$ (Pa/m)	k_2' ($m^{-2}s^{-1}$)
(6,6)	1.16(±0.03)E-14	3.386E+13	2.91(±0.06) E+27
(7,7)	3.97(±0.18)E-15	7.6941E+13	1.94(±0.09) E+28
(8,8)	1.05(±0.06)E-14	1.0321E+14	9.85(±0.55) E+27
(10,10)	1.46(±0.06)E-14	2.0456E+14	1.40(±0.06) E+28
(15,15)	3.81(±0.08)E-14	2.1736E+14	5.71(±0.12) E+27
(30,30)	2.21(±0.06)E-13	2.2915E+14	1.04(±0.03) E+27

Table 11 Results for BNNT q=±0.3e

Chirality	$\dot{m}$ (kg/s)	$\Delta P/\Delta L$ (Pa/m)	k_2' ($m^{-2}s^{-1}$)
(6,6)	1.16(±0.03)E-14	3.386E+13	2.91(±0.06) E+27
(7,7)	3.97(±0.18)E-15	7.6941E+13	1.94(±0.09) E+28
(8,8)	1.05(±0.06)E-14	1.0321E+14	9.85(±0.55) E+27
(10,10)	1.46(±0.06)E-14	2.0456E+14	1.40(±0.06) E+28
(15,15)	3.81(±0.08)E-14	2.1736E+14	5.71(±0.12) E+27
(30,30)	2.21(±0.06)E-13	2.2915E+14	1.04(±0.03) E+27

Table 12 Results for BNNT q=±0.6e

Chirality	$\dot{m}$ (kg/s)	$\Delta P/\Delta L$ (Pa/m)	k_2' ($m^{-2}s^{-1}$)
(6,6)	9.09(±0.10)E-15	7.9693E+14	8.77(±0.28) E+28
(7,7)	7.51(±0.14)E-15	8.9104E+14	1.19(±0.04) E+29
(8,8)	1.67(±0.22)E-14	5.1558E+14	3.09(±0.15) E+28
(10,10)	4.20(±0.03)E-14	2.56E+15	6.11(±0.10) E+28
(15,15)	5.21(±0.06)E-14	1.09E+15	2.09(±0.07) E+28
(30,30)	1.30(±0.05)E-13	4.0235E+14	3.09(±0.10) E+27

Table 13 Results for BNNT q=±0.959e

Chirality	$\dot{m}$ (kg/s)	$\Delta P/\Delta L$ (Pa/m)	k_2' ($m^{-2}s^{-1}$)
(6,6)	1.49(±0.01)E-14	3.39E+15	2.28(±0.02) E+29
(7,7)	1.30(±0.01)E-14	3.90E+15	3.01(±0.03) E+29
(8,8)	9.85(±0.22)E-14	5.16E+15	5.23(±0.12) E+28
(10,10)	3.41(±0.03)E-14	5.13E+15	1.50(±0.01) E+29
(15,15)	1.21(±0.01)E-13	5.44E+15	4.51(±0.02) E+28
(30,30)	1.59(±0.50)E-14	1.1466E+14	7.23(±2.26) E+27

2.3 Pore edge configurations

We studied a number of pore edge configurations for the (10,10) nanotube. The configurations, along with the density profiles generated by them, are shown in Fig. 2. For some of the configurations, we either hydrogenated the edge of the BN sheet, or the nanotube, or both the sheet edge and nanotube. Where the edges are hydrogenated, the partial charges on the membrane are set by running a charge equilibration scheme as outlined in section 1.3. As can be observed from Fig. 2, most of the configurations reduce the high concentration of density which appeared in the setup that did not have any modification. The smoothest density contours was achieved by setting all partial charges to zero. The next best was achieved by hydrogenating all the pore edges. This also reflects in the end resistance, with the end resistance of the zero partial charge BNNT being the lowest.

While most of the hydrogenated BNNT configurations have nearly similar end resistance as the case with no partial charges, some configurations do have a high end resistance, which should be avoided to avoid spurious high end resistance values while studying these membranes using MD simulations.

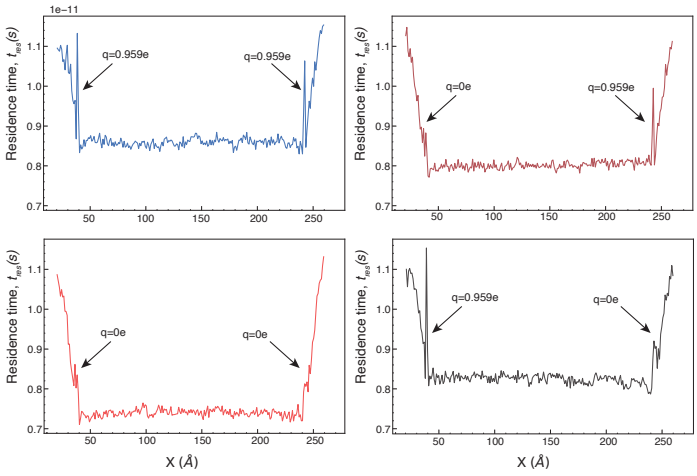

Fig. 3 Residence time for (15,15) nanotube in setup 1, with edge treatments at different locations. The charge on the nanotube remained the same q = ±0.959e for all four cases. Wherever q = 0e on some membranes, the residence time at that location is seen to drop, and also the overall residence time of the flow inside the tube.

2.4 Residence time

The residence time for setup 1 was studied for some of the configurations introduced in section 2.3. For studying the effectiveness of the edge treatments described in the above section, we removed the charges from the sheet at only one pore edge alternatively. There was a difference in the local residence time depending on which end had been treated, shown in Fig. 3.

2.5 Droplet simulations

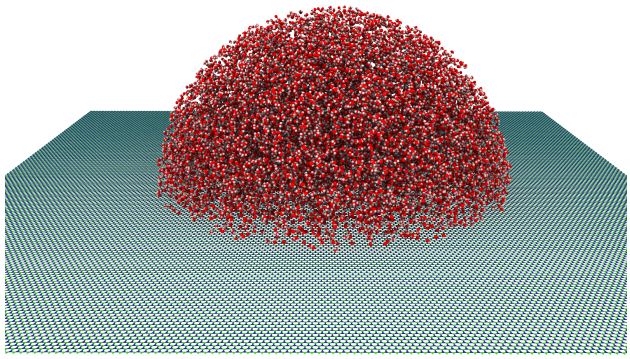

Fig. 4 Simulation snapshot for the droplet study.

A droplet was simulated on a single layer graphene sheet and BN sheet, shown in Fig. 4. The droplet consists of 17511 water molecules, and is large enough to produce a macroscopic contact angle value. The droplet was initialised as a hemisphere sitting one water molecule diameter away from the desired surface. The temperature of the droplet was maintained at 300 K using a Berendsen thermostat, and the simulation was carried out in the NVE ensemble. We studied different partial charges on the BN sheet, and found no significant changes in the contact angle. The results are presented in Fig. 5.

Since we did not observe significant variation in the contact angle with changes in partial charges, we kept the LJ parameters constant for all of our simulations.

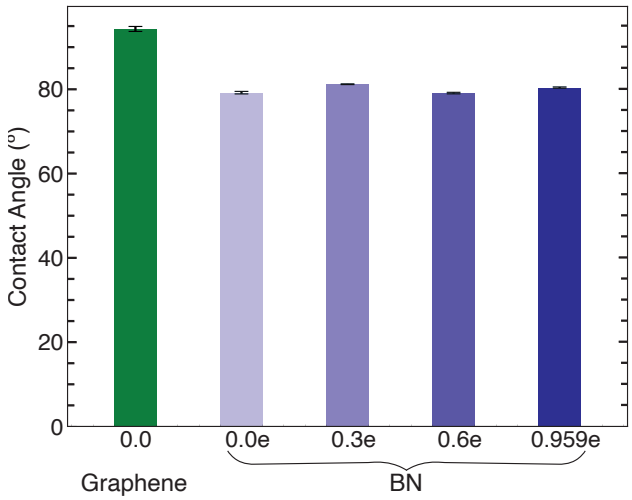

Fig. 5 Contact angles from the droplet simulations. Change in partial charge q between $0 - \pm 0.959$e did not show any changes in the contact angle.

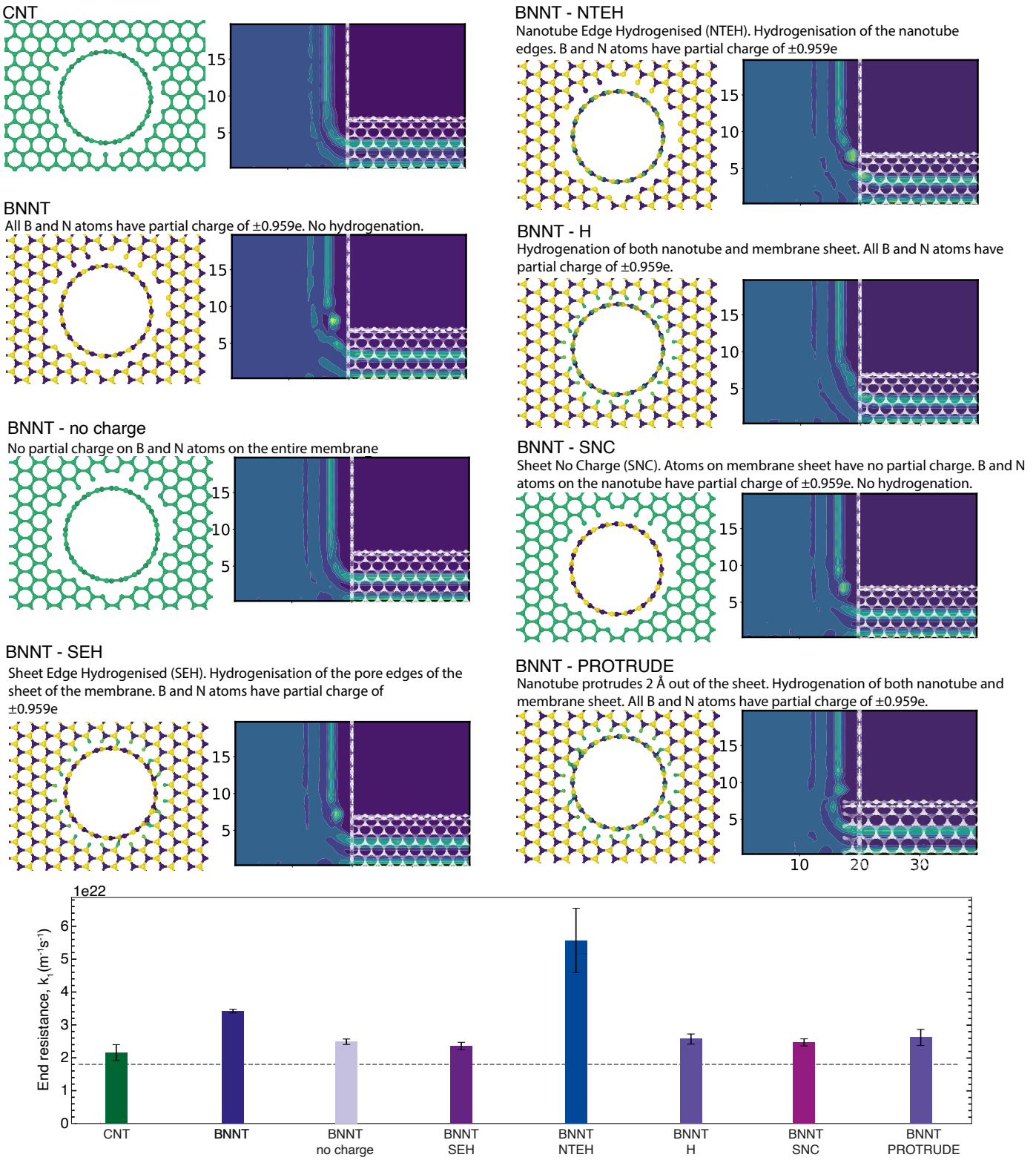

Fig. 2 Description of the various end configurations alongside their density plots. End resistance for the configurations at the bottom. Most of the edge configurations resulted in only slightly higher end resistances than the CNT.

2.6 Slip length

Slip lengths from our current studies are compared to values from the literature in Fig. 6. These slip lengths are calculated using the Hagen-Poiseuille equation, but require other parameters such as viscosity and density, and therefore slip length alone does not present the complete picture of flows inside nanotubes.

Partial charges do affect the slip (and the nanotube flow resistance) significantly. Larger slip lengths are observed in BNNTs with no partial charge when compared to CNTs with no partial charges. This does not necessarily indicate that a BNNT with no partial charges would have higher slip, as the true partial charges, and the van der Waals interaction parameters in real BNNT membranes, especially at small diameters, are still unclear.

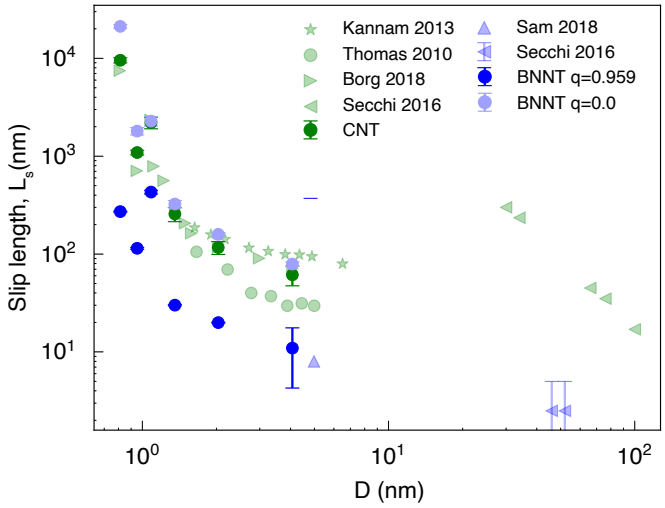

Fig. 6 Slip lengths for nanotubes. BNNTs with no partial charges show a significant increase in slip length.

The viscosity and density values used to calculate the slip length are presented in Table 14. The viscosity values used are empirical values obtained from Borg *et al.*[3]

Table 14 Viscosity and density inside BNNT and CNT nanotubes

Chirality	μ (Pa.s)	ρ (kg/m^3)
(6,6)	0.000870	601.97
(7,7)	0.001175	678.73
(8,8)	0.001790	901.19
(10,10)	0.000890	897.06
(15,15)	0.000855	955.63
(30,30)	0.000855	1000.87

2.7 Potential energy field

The potential energy surface felt by an oxygen atom close to the surface of a (30,30) BNNT is shown in Fig. 7 and Fig. 8. The potential energy surface for BNNT with $q = \pm 0.959$e is more uneven, with deeper troughs and higher crests compared to one with q = 0e. This increase in the roughness of the potential energy field due to the presence of partial charges contributes to the increasing nanotube flow resistance k_2' with increasing partial charge. This increase in roughness resembles the findings of Wei *et al.*[13] for CNTs with an artificial partial charge.

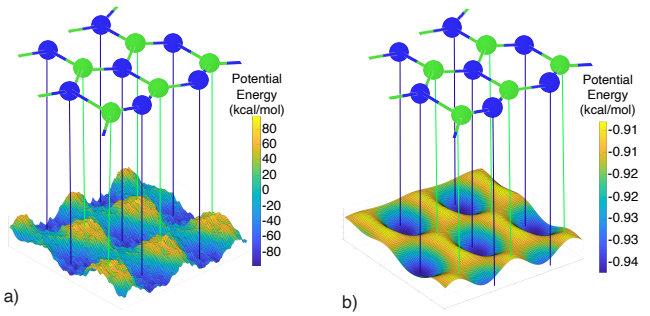

Fig. 7 Potential energy landscape for (30,30) BNNTs with partial charge q = a) ± 0.959e and b) 0e

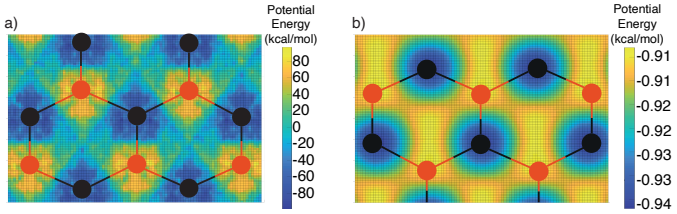

Fig. 8 Top view of the potential energy landscape for (30,30) BNNTs with partial charge q = a) ± 0.959e and b) 0e.

3 Literature data

The data obtained from literature is provided in Tables 15 and 16. Where this was unavailable, data has been extracted from the figures.

Table 15 Data obtained from literature for flows through BNNT and CNT membranes using MD simulations.

Study	ΔP (MPa)	Flow rate (m^3/s)	Diameter (nm)	Material	Length (Å)	Resistance ($m^{-1}s^{-1}$)
Suk 2008[21]	100	3.80E-16	0.83	BNNT	14	2.62E+23
	200	7.11E-16	0.83		14	2.80E+23
	300	9.47E-16	0.83		14	3.16E+23
	400	1.15E-15	0.83		14	3.46E+23
	500	1.46E-15	0.83		14	3.41E+23
	100	3.20E-16	0.81	CNT	14	3.12E+23
	200	5.64E-16	0.81		14	3.54E+23
	300	8.98E-16	0.81		14	3.33E+23
	400	1.06E-15	0.81		14	3.74E+23
	500	1.33E-15	0.81		14	3.73E+23
Hilder 2009[7]	60.73	1.96E-16	0.69	BNNT	14	3.09E+23
	152.60	5.41E-16	0.69	(q=0.4e)	14	2.81E+23
	244.46	6.13E-16	0.69		14	3.98E+23
	305.47	6.57E-16	0.69		14	4.64E+23
	366.48	8.25E-16	0.69		14	4.43E+23
	458.35	8.69E-16	0.69		14	5.27E+23
	611.92	1.35E-15	0.69		14	4.50E+23
	60.64	4.12E-17	0.69	BNNT	14	1.46E+24
	152.48	9.06E-17	0.69	(q=1.05e)	14	1.68E+24
	243.67	4.30E-17	0.69		14	5.66E+24
	305.33	1.48E-16	0.69		14	2.06E+24
	367.07	8.94E-17	0.69		14	4.10E+24
	458.18	1.91E-16	0.69		14	2.39E+24
	611.76	1.87E-16	0.69		14	3.25E+24
Zhang 2019[15]	50	6.08E-16	1.09	BNNT	50	8.21E+22
	100	1.32E-15	1.09		50	7.52E+22
	150	1.83E-15	1.09		50	8.18E+22
	200	2.44E-15	1.09		50	8.18E+22
	250	3.04E-15	1.09		50	8.20E+22
Casanova 2020[14]	1.66	3.48E-15	4.068	BNNT	20.4	4.76E+20
	10.61	2.22E-14	4.068		20.4	4.77E+20
	1.65	4.20E-15	4.068	CNT	20.4	3.91E+20
	10.68	2.71E-14	4.068		20.4	3.92E+20
Liang 2017[8]	10	1.49E-16	0.66	BNNT	50	6.68E+22
	100	1.74E-16	0.66		50	5.72E+23
	200	5.57E-16	0.66		50	3.59E+23
	300	6.85E-16	0.66		50	4.37E+23
	400	1.18E-15	0.66		50	3.37E+23
	500	1.41E-15	0.66		50	3.52E+23
	10	1.85E-16	0.81	BNNT	50	5.38E+22
	100	5.93E-16	0.81		50	1.68E+23
	200	9.26E-16	0.81		50	2.15E+23
	300	1.30E-15	0.81		50	2.29E+23
	400	1.49E-15	0.81		50	2.66E+23
	500	1.82E-15	0.81		50	2.74E+23
	10	1.88E-16	0.93	BNNT	50	5.29E+22
	100	8.24E-16	0.93		50	1.21E+23
	200	1.41E-15	0.93		50	1.41E+23
	300	2.18E-15	0.93		50	1.37E+23
	400	2.87E-15	0.93		50	1.39E+23
	500	3.40E-15	0.93		50	1.46E+23
	10	2.46E-16	1.09	BNNT	50	4.04E+22
	100	1.02E-15	1.09		50	9.73E+22
	200	1.69E-15	1.09		50	1.17E+23
	300	2.70E-15	1.09		50	1.11E+23
	400	3.72E-15	1.09		50	1.07E+23
	500	4.21E-15	1.09		50	1.18E+23

Table 16 Data obtained from literature for flows through membranes using MD simulations (cont.)

Study	ΔP (MPa)	Flow rate (m^3/s)	Diameter (nm)	Material	Length (Å)	Resistance ($m^{-1}s^{-1}$)
Borg 2018[3]	200	7.5E-16	0.81	CNT	200	2.66E+23
	200	1.84E-15	0.95		200	1.08E+23
	200	1.8E-15	1.08		200	1.11E+23
	200	2.51E-15	1.11		200	7.96E+22
	200	4.9E-15	1.22		200	4.08E+22
	200	8.96E-15	1.36		200	2.23E+22
	200	1.40E-14	1.49		200	1.42E+22
	200	1.80E-14	1.58		200	1.10E+22
	200	4.68E-14	2.03		200	4.26E+21
	200	1.82E-13	2.98		200	1.09E+21
	200	5.09E-13	4.07		200	3.92E+20
Corry 2007[23]	208	3.10E-16	0.66	CNT	14	6.68E+23
	208	6.96E-16	0.81		14	2.98E+23
	208	1.30E-15	0.93		14	1.59E+23
	208	2.43E-15	1.09		14	8.53E+22
Ritos 2014[10]	200	6.50E-14	2.034	CNT	5.38E+02	3.07E+21
	200	6.84E-14	2.034		2.56E+02	2.92E+21
	200	6.54E-14	2.034		1.27E+02	3.06E+21
	200	6.81E-14	2.034		5.07E+01	2.94E+21
	200	7E-14	2.034		2.53E+01	2.86E+21
	200	1.52E-14	2.072	BNNT	4.96E+02	1.31E+22
	200	2.27E-14	2.072		2.47E+02	8.81E+21
	200	2.89E-14	2.072		1.24E+02	6.90E+21
	200	2.57E-14	2.072		4.97E+01	7.76E+21
	200	3.15E-14	2.072		2.48E+01	6.34E+21

Notes and references

1 S. Plimpton, *Journal of Computational Physics*, 1995, **117**, 1–19.

2 E. Lemmon, M. McLinden and D. Friend, *Thermophysical Properties of Fluid Systems*, 2017.

3 M. K. Borg, D. A. Lockerby, K. Ritos and J. M. Reese, *Journal of Membrane Science*, 2018, **567**, 115–126.

4 S.-P. Ju, Y.-C. Wang and T.-W. Lien, *Nanoscale Research Letters 2011 6:1*, 2011, **6**, 1–11.

5 C. Y. Won and N. R. Aluru, *Journal of the American Chemical Society*, 2007, **129**, 2748–2749.

6 C. Y. Won and N. R. Aluru, *Journal of Physical Chemistry C*, 2008, **112**, 1812–1818.

7 T. A. Hilder, D. Gordon and S. H. Chung, *Small*, 2009, **5**, 2183–2190.

8 L. Liang, J. C. Li, L. Zhang, Z. Zhang, J. W. Shen, L. Li and J. Wu, *Physical Chemistry Chemical Physics*, 2017, **19**, 30031–30038.

9 A. Sam, R. Hartkamp, S. K. Kannam and S. P. Sathian, *Nanotechnology*, 2018, **29**, 485404.

10 K. Ritos, D. Mattia, F. Calabrò and J. M. Reese, *Journal of Chemical Physics*, 2014, **140**, 014702.

11 T. A. Hilder, R. Yang, V. Ganesh, D. Gordon, A. Bliznyuk, A. P. Rendell and S. H. Chung, *Micro and Nano Letters*, 2010, **5**, 150–156.

12 Y. Wu, L. K. Wagner and N. R. Aluru, *Journal of Chemical Physics*, 2016, **144**, 164118.

13 X. Wei and T. Luo, *Journal of Physical Chemistry C*, 2018, **122**, 5131–5140.

14 S. Casanova, S. Mistry, S. Mazinani, M. K. Borg, Y. M. Chew and D. Mattia, *Nanoscale*, 2020, **12**, 21138–21145.

15 L. Zhang, L. Jia, J. Zhang, J. Li, L. Liang, Z. Kong, J. W. Shen, X. Wang, W. Zhang and H. Wang, *Desalination*, 2019, **464**, 84–93.

16 H. M. Aktulga, J. C. Fogarty, S. A. Pandit and A. Y. Grama, *Parallel Computing*, 2012, **38**, 245–259.

17 S. S. Han, J. K. Kang, H. M. Lee, A. C. Van Duin and W. A. Goddard, *Journal of Chemical Physics*, 2005, **123**, 114703.

18 J. L. Abascal and C. Vega, *Journal of Chemical Physics*, 2005, **123**, 234505.

19 H. C. Andersen, *Journal of Computational Physics*, 1983, **52**, 24–34.

20 R. W. Hockney and J. W. Eastwood, *Computer Simulation Using Particles*, A. Hilger, 1988.

21 M. E. Suk, A. V. Raghunathan and N. R. Aluru, *Applied Physics Letters*, 2008, **92**, 133120.

22 H. J. Berendsen, J. P. Postma, W. F. Van Gunsteren, A. Dinola and J. R. Haak, *The Journal of Chemical Physics*, 1984, **81**, 3684–3690.

23 B. Corry, *Journal of Physical Chemistry B*, 2008, **112**, 1427–1434.